Chapter 4

Ultrasonic Assisted Machining of Nickel-Based Superalloy Inconel 718

Yongbo Wu, Qiang Wang, Sisi Li and Dong Lu

Additional information is available at the end of the chapter

http://dx.doi.org/10.5772/intechopen.76085

Abstract

Inconel 718 has been widely used in industries because of its excellent mechanical properties. However, the machining process, particularly the turning/grinding, of Inconel 718 is still costly due to high cutting force and heavy tool damage. Fortunately, a promising material removal technique, that is, ultrasonic-assisted turning/grinding (called UAT/UAG for simplicity), could potentially play a great role in the high efficiency precision machining of Inconel 718 due to its excellent features such as smaller turning/grinding force, better surface quality, longer tool working life and lower heat generation. However, few attempts have been done on UAT/UAG of Inconel 718. Therefore, in this work, in order to confirm the feasibility of machining Inconel 718 by UAT/UAG, experimental apparatus/equipment has at first been constructed by installing an ultrasonic cutting-unit/spindle on a NC lathe/surface grinder for UAT/UAG operations, and then experimental investigations have been performed to elucidate the fundamental machining characteristics involving Inconel 718 workpiece including the effects of the ultrasonic vibration and the cutting/grinding speed on the work-surface finish, the machining force and temperature, the chip formation, the tool/wheel wears and so on. The obtained results show that grinding forces and surface roughness were decreased in UAT/UAG.

Keywords: Inconel 718, machining, turning, grinding, ultrasonic vibration, surface roughness, material removal, chip formation

1. Introduction

Inconel 718, a nickel-based superalloy, exhibits desirable properties over a wide temperature range and is widely used in aerospace, petroleum and nuclear industries because of

its excellent mechanical properties such as high fatigue strength, good corrosion resistance and strong creep resistance [1]. In power generation equipment manufacturing industries including gas turbine engines, most of Inconel 718-made products are commonly machined by turning, cutting, milling and grinding. However, the excellent mechanical properties of Inconel 718 are leading to high cutting force, severe work-surface damage and heavy tool wear in conventional machining/finishing processes [2]. Especially, the turning/grinding process (hereinafter called CT/CG for simplicity) of Inconel 718 is still costly due to the heavy and rapid wear of tools.

As a promising material removal technique, ultrasonic-assisted turning/grinding (hereinafter called UAT/UAG for simplicity) has attracted great attention for decades for the sake of its excellent features such as smaller turning/grinding force, higher material removal rate, better surface quality, longer tool working life and lower heat generation compared with those in CT/CG [3–7]. However, in the most of conventional UAT processes, a linear ultrasonic vibration is applied only in a single direction [8–12], which leads to the difficulty in the obtainment of a reasonable material removal rate especially for difficult-machine metal such as Inconel 718. On the other hand, in conventional UAG processes, most of researches have ever focused mainly on the hard-brittle materials such as crystal silicon and ceramics [13–19], and few attempts have been done involving Inconel 718.

Therefore, the present authors proposed a novel UAT technique in which an elliptical ultrasonic vibration generated by the synthesis of two orthogonal linear ultrasonic vibrations is applied on the tool in the base plane and experimentally confirmed its performance in the turning of Inconel 718 [20, 21]. This new method is hereafter called as EUAT. In addition, the UAG of Inconel 718 in which a linear ultrasonic vibration is imposed to the grinding wheel along the wheel axis was also attempted, and some significant results were attained [22, 23]. In this chapter, the processing principles of EUAT/UAG and the respective corresponding apparatuses are described. Then, the fundamental machining characteristics obtained are detailed.

2. Elliptical ultrasonic-assisted turning of Inconel 718

2.1. Processing principle and apparatus

The processing principle of elliptical ultrasonic-assisted turning (EUAT) is as illustrated in **Figure 1**; an elliptical ultrasonic vibration is imposed on the cutting tool in the base plane (XOY plane) and the workpiece is rotated at a speed n_w around its own axis (X-axis) in addition to a feed motion of the cutting tool in X-direction at a feed rate v_f and a depth of cut a_p. The elliptical ultrasonic vibration is achieved by the synthesis of two vibrations in X- and Y-directions with the respective amplitudes of A_x and A_y generated simultaneously by the ultrasonic vibration unit.

For realizing the processing principle, an experimental apparatus was constructed by installing a commercial ultrasonic vibration unit (UL40-A1 by Takesho Co., Ltd.) onto the

http://dx.doi.org/10.5772/intechopen.76085

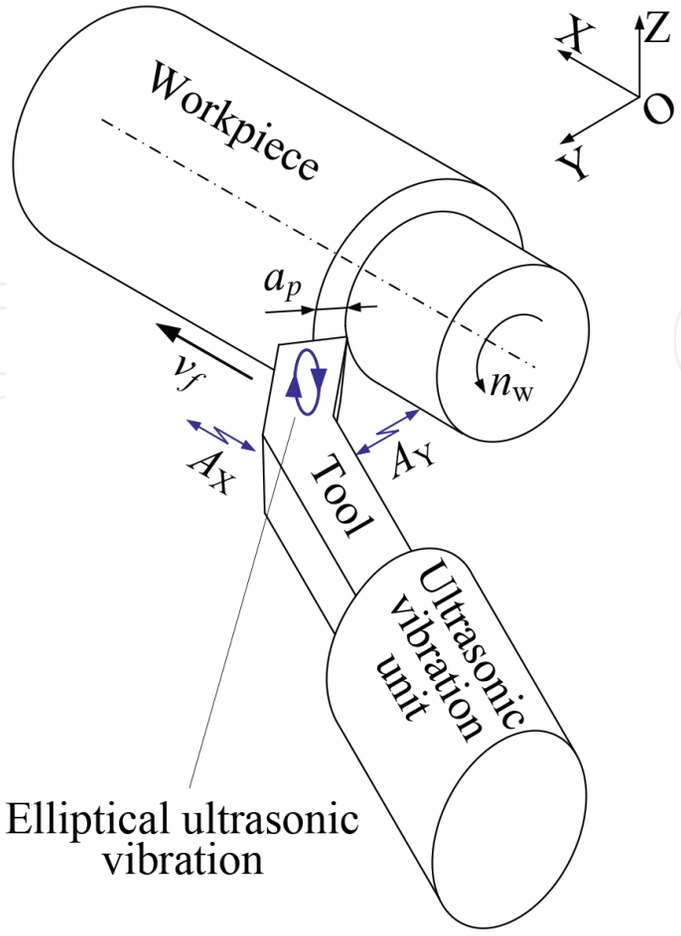

Figure 1. Processing principle of EUAT.

tool post of a commercial CNC lathe (TAC-360 by Takizawa Co., Ltd.) as shown in **Figure 2**. A power supplier was used to apply an AC voltage into the ultrasonic unit for inducing the ultrasonic vibration. A commercial dynamometer was fixed below the ultrasonic unit to measure the cutting forces. As the tool, a coated carbide insert, which is installed at the tip of the ultrasonic unit, was employed. The cutting temperature was measured using an infrared camera.

For quantitatively confirming the generation of elliptical vibration, the vibrations of tool cutting edge in *X*- and *Y*-directions were simultaneously measured by two laser Doppler vibrometers (LV-1610; Ono Sokki Co., Ltd.). The frequency of the AC voltage was set at 40.9 kHz, based on the given specification of the ultrasonic unit. **Figure 3** plots the vibration amplitudes of the tool cutting edge, A_x in X-direction and A_y in Y-direction, at different power supplying levels. It is evident that as the power supplying increases, the values of A_x and A_y increase linearly to 2.35 and 2.05 μm, respectively, at the power level of 40%. Using the vibrations measured in both directions, the trajectory of the tool cutting edge was captured by an oscilloscope (WaveJet 314; LeCroy Co., Ltd), and the obtained trajectories for different power supplying levels were also exhibited in **Figure 3**. Clearly, the tool cutting edge follows a clockwise elliptic motion, and the

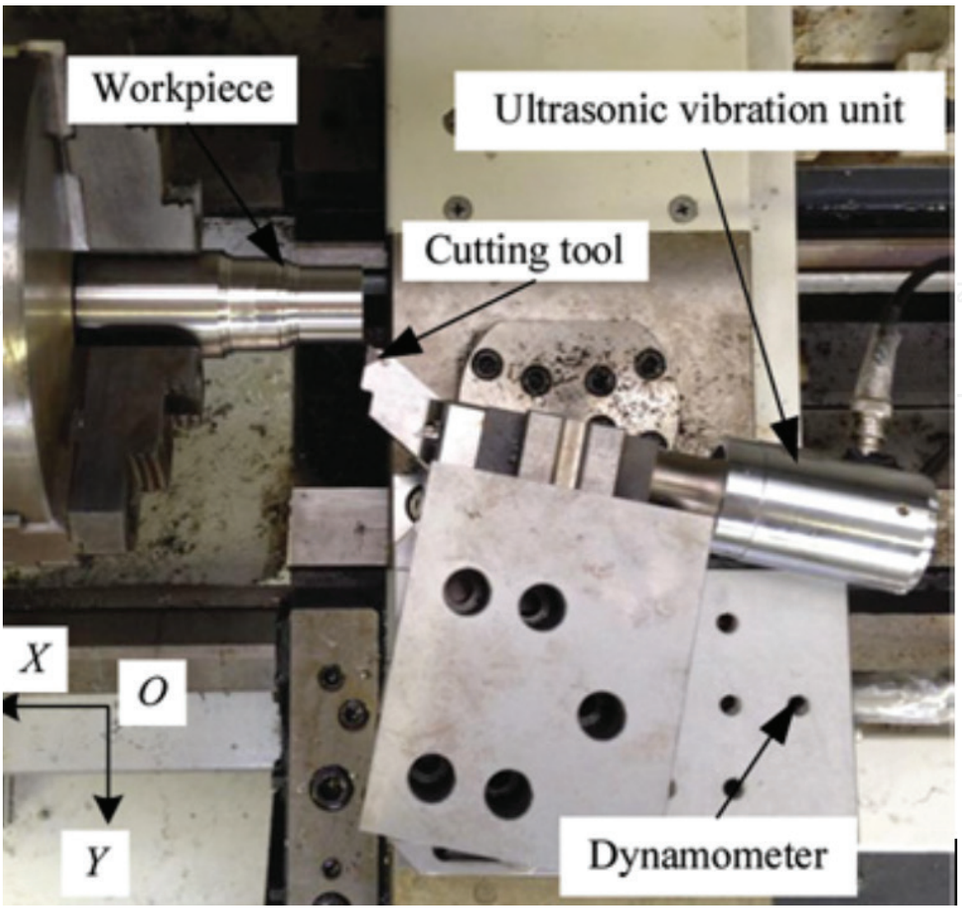

Figure 2. Apparatus for EUAT.

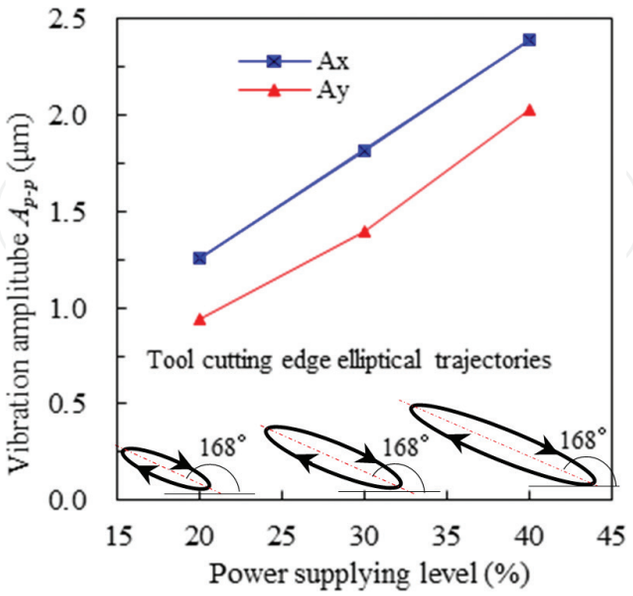

Figure 3. Effect of power supplying level on vibration amplitude.

shape of ellipse remains essentially unchanged with a declined angle of 168° even the power supplying level varied, but the size of trajectory increased as the power supplying level escalated.

2.2. Machining conditions and procedure

Table 1 summarizes the machining conditions in experiments. As the workpiece, an Inconel 718 rod with the dimension of 40 mm in diameter and 100 mm in length was used. The cutting speed v_c was hence changed from 75 m/min to 125 m/min when the workpiece rotational speed n_w was adjusted from 600 to 1000 rpm. During machining, the cutting forces and the cutting temperature were measured using the three-component dynamometer and the infrared camera, respectively. After machining, the work-surface roughness was evaluated by using a surface profiler (Talysurf Intra by Taylor Hobson Inc.), and the surface morphology of workpiece was captured by using a laser microscope (VK-8710 by Keyence Co., Ltd). In addition, for comparison, the conventional turning (CT) operations were also conducted on the same experimental apparatus but turned off the power supplier to set the power supplying level at 0%, that is, $A_x = A_y = 0$.

2.3. Fundamental machining characteristics

Cutting force and temperature. In order to confirm that the ultrasonic vibration-reducing effect of cutting force (UREF) still exists in the high speed cutting of Inconel 718 when EUAT is performed in the base plane, the effect of cutting speed on cutting force in CT and EUAT was studied by experiments. The results are presented in **Figure 4**, demonstrating that in comparison with CT with EUAT, when the cutting speed was 75 m/min, the feed force F_x, the radial force F_y and the cutting force F_z were reduced by 38%, 46% and 25%, respectively. Similarly, even the cutting speed was increased to 87.5 m/min, then 100 m/min, further 112.5 m/min and finally 125 m/min, similar reduction percentages were observed on the F_x, F_y and F_z with those at 75 m/min.

In other words, even when the cutting speed goes beyond the maximum ultrasonic vibration velocity of $\pi f A_{p\text{-}p}$, UREF is barely affected by the increase in the cutting speed. This may be

Workpiece	Inconel 718 (φ 40 mm × L 100 mm)
Cutting tool	Coated carbide
	Normal rake angle α = 0 (°)
	Normal clearance angle γ = 11 (°)
	Nose radius r_n = 0.4 rn(mm)
Cutting parameters	n_w = 600–1000 (rpm) (v_c = 75–125 m/min), v_f = 0.05 (mm/rev), a_p = 0.05 (mm)
Ultrasonic vibration	In CT: $A_x = A_y = 0$
	In EUAT: f = 40.9 kHz, A_x = 2.07 μm, A_y = 2.81 μm, declined angle: 168°
Coolant	Dry cutting

Table 1. Machining conditions in EUAT of Inconel 718.

because the ultrasonic separation exists between the tool nose and the workpiece in X- and Y-directions in the base plane, respectively, in EUAT. In addition, in both CT and EUAT, the largest force was F_y, followed by F_x and F_z in descending order [24].

The cutting temperatures at different cutting speeds in CT and EUAT were also obtained as shown in **Figure 5**. The results demonstrated that either in CT or in EUAT, as the cutting speed increased, the cutting temperature rose monotonously; however, the increase rate in EUAT seemed consistently lower than that in CT, indicating the ultrasonic vibration significantly contributed to the reduction of cutting temperature in turning Inconel 718.

Chip morphology. Figure 6 shows that the chip width in EUAT is smaller than that in CT, indicating that the chip morphology is affected by the cutting forces; the increase in cutting force adds the transverse flow of the material, leading to an increase in the chip width [25]. Moreover, the adhesion of microchips can be observed evidently on the chip surface in CT, which can hardly be seen in EUAT. These phenomena may be connected to the formation of BUE (built-up edge) during cutting, which will be discussed in the "Tool Wear" section.

Work-surface finish. The surface morphologies of workpieces machined by CT and EUAT at three different cutting speeds of 75, 100 and 125 m/min were captured by the laser microscope. From the microscopic images shown in **Figure 7(a)**, it is found that regardless of the cutting speed, obvious parallel cutting traces and randomly distributed pits can be observed on the work-surface in CT; the phenomena may be attributed to the formation of BUE on the cutting tool and chip winding during cutting. By contrast, in EUAT (**Figure 7(b)**), knitted work-like texture was formed on the work-surface owing to the tool vibration, and the work-surface integrity became better. This is probably attributed to the fact that the chips were no longer wrapped around workpiece and easily broken for the sake of the elliptical vibration of cutting tool in the base plane.

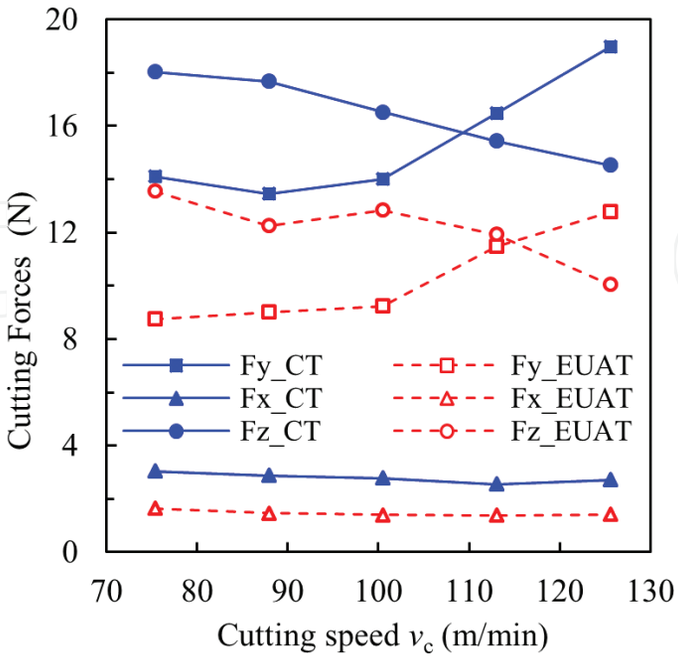

Figure 4. Effect of cutting speed on cutting forces.

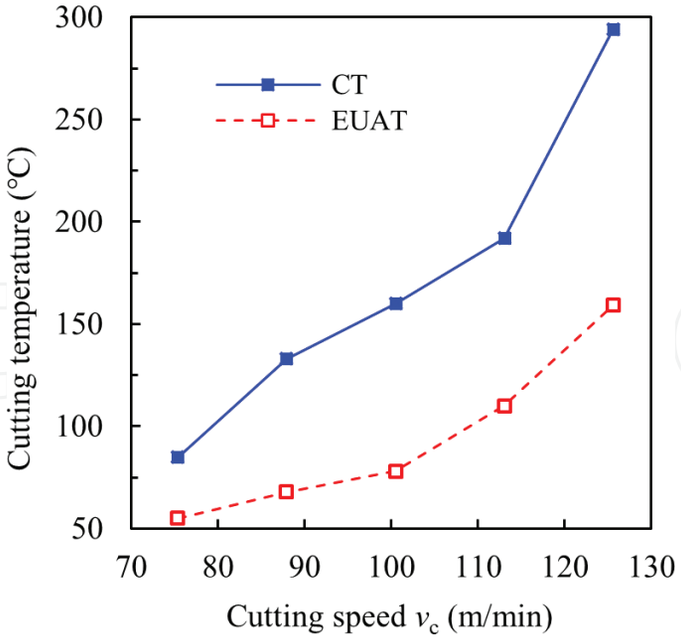

Figure 5. Effect of cutting speed on cutting temperatures.

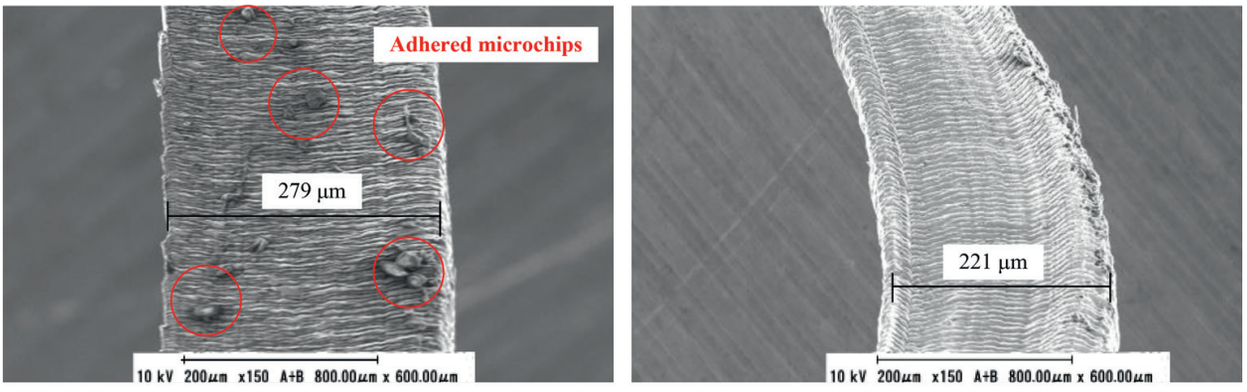

Figure 6. SEM micrographs of chips developed in CT and EUAT methods: (a) in CT and (b) in EUAT.

The work-surface roughness was measured in the feed direction using the surface profiler for both CT and EUAT. The evaluation length was set to 5 mm. In each test, the surface roughness parameters R_a and R_z were measured eight times, and their average values were calculated and regarded as the roughness. **Figure 8** shows the effect of the cutting speed on the work-surface roughness in CT and EUAT at three different cutting speeds of 75, 100 and 125 m/min. The surface roughness R_a and R_z in EUAT seemed both larger than those in CT. In EUAT with the increase of cutting speed, the R_a and R_z slightly decreased, while in CT, the R_a and R_z tended to increase slightly which is caused by the formation of built-up edge (BUE) on tool cutting edge [20].

Tool wear. Figure 9(a) and **(b)** shows the SEM images of the cutting edge of tool employed for 4.2 min in CT and EUAT, respectively. Evidently, in CT, the BUE appeared on the cutting

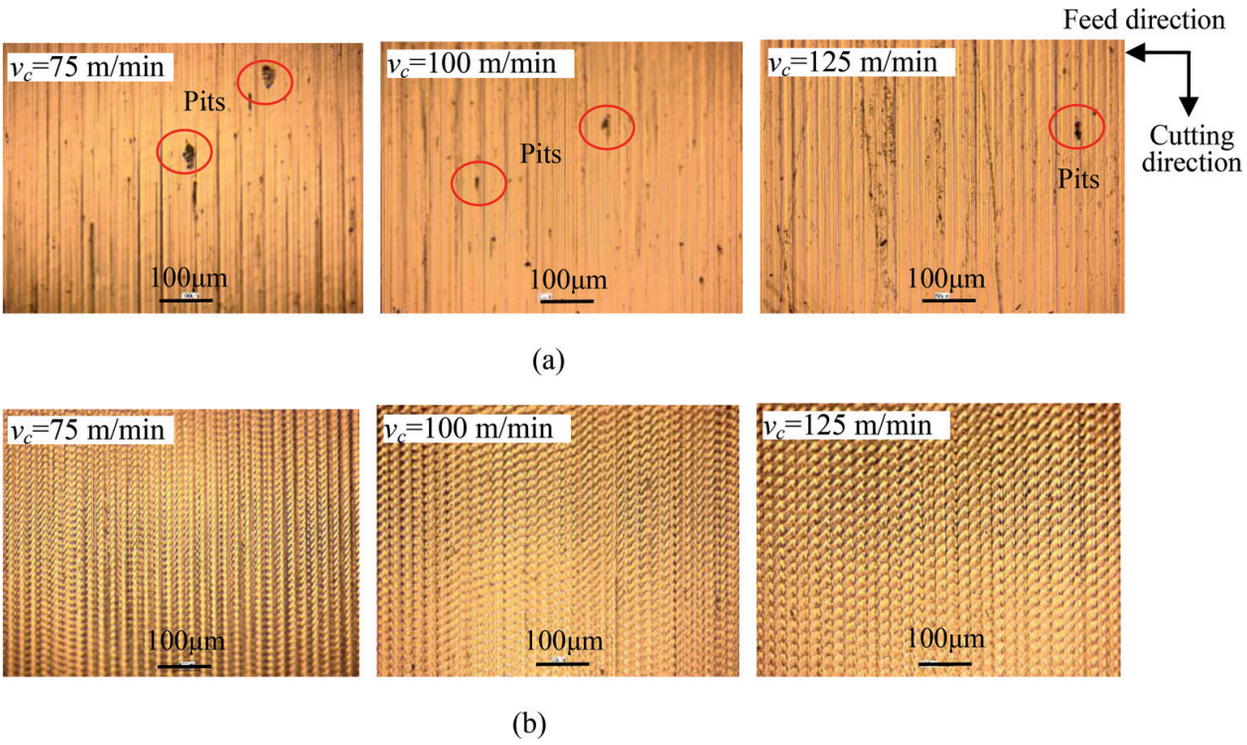

Figure 7. 2D laser microscopic images of the work-surfaces machined: (a) in CT and (b) in EUAT.

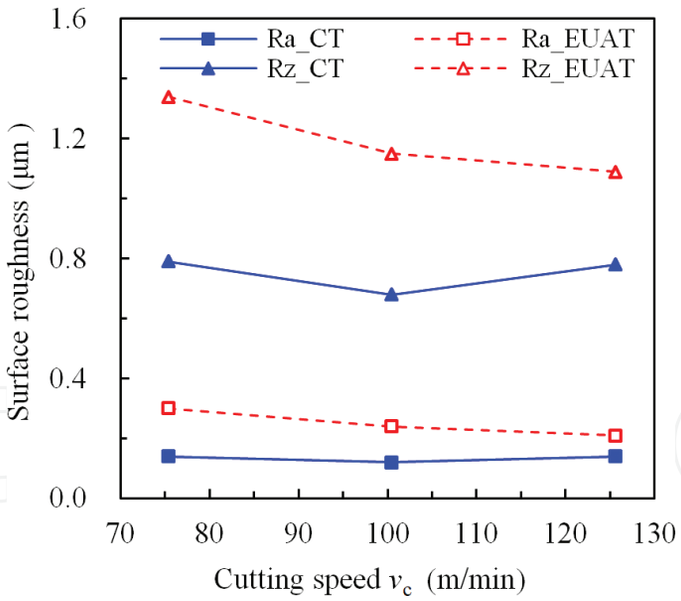

Figure 8. Effect of cutting speed on work-surface roughness.

tool, whereas in EUAT, it was absent. Comparing **Figure 9(a)** with **Figure 9(b)** shows that the cutting tool adopted in CT experienced considerably heavier flank wear than that adopted in EUAT. The maximum flank wears in CT and EUAT were 0.23 and 0.19 mm, respectively. This indicates that the cutting tool was worn down more rapidly in CT than in EUAT, possibly because the tool vibration in EUAT reduces the friction between the tool and the workpiece. In EUAT, the ultrasonic vibration of tool occurs simultaneously in X- and Y-directions and

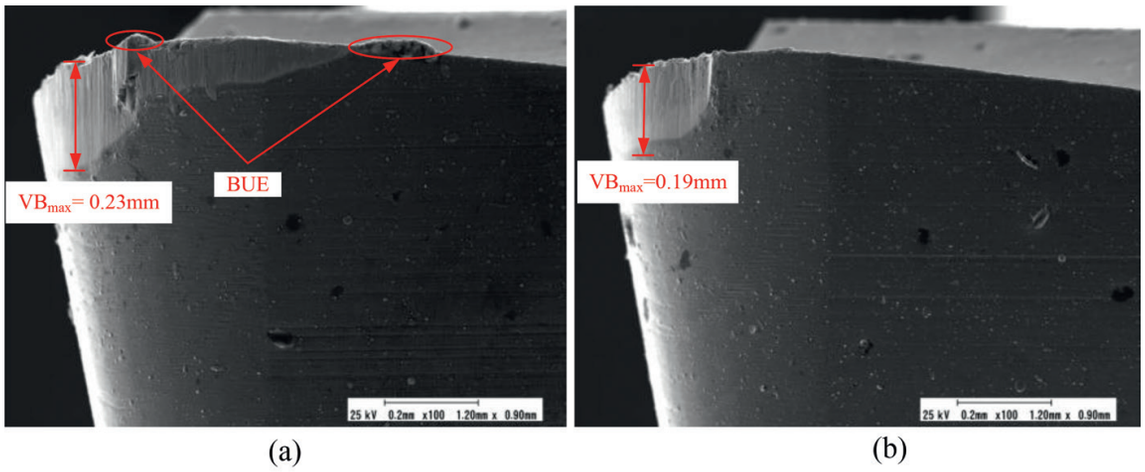

Figure 9. SEM images of cutting tools used in (a) CT and (b) EUAT for 4.2 min (power supply level = 20%).

results in a clockwise elliptical motion in the base plane (see **Figure 1**). During cutting, owing to the elliptic vibration the tool repeats the cutting-in and cutting-out action periodically. This action reduces the formation of BUE and eventually retains the sharpness of the tool cutting edge. Therefore, the chips and the work-surface in EUAT are almost free of chip particles.

3. Ultrasonic-assisted grinding of Inconel 718

3.1. Processing principle and equipment

The processing principle of UAG is illustrated in **Figure 10**; an axial ultrasonic vibration is imposed on the grinding wheel in x-direction and the workpiece is fixed on a work-holder under which a z-stage is located for determining the wheel depth of cut Δ. The peripheral speed of grinding wheel is V_c and a feed motion is given to the workpiece in y-direction. For comparison, a conventional grinding (CG) was also performed by releasing spindle from ultrasonic vibration (**Figure 11**).

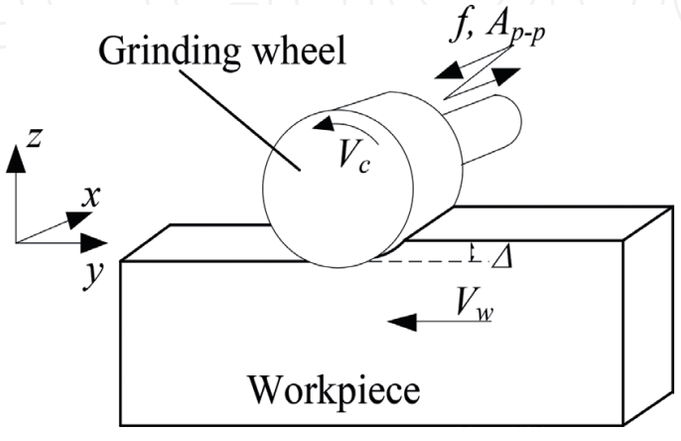

Figure 10. Processing principle of ultrasonic-assisted grinding.

For realizing the processing principle, an experimental apparatus was constructed by installing a commercial ultrasonic vibration spindle (URT40 by Takesho Co., Ltd., Japan) onto a commercial NC grinder (GRIND-X IGM15EX by Okamoto Machine Tool Co., Ltd., Japan). A commercial dynamometer (9256A by Kistler Co., Ltd., Switzerland) was positioned under the ultrasonic spindle. On the lower end of the spindle, a metal-bonded #140 cBN grinding wheel with a diameter of d_s = 8 mm was fixed and an Inconel 718 specimen (L48 mm×W36 mm×T3 mm) was used as the workpiece. The abrasive grains on the working surface of the wheel employed were observed by a three-dimensional (3D) SEM (ERA-8900 by ELIONIX. Co., Ltd., Japan), showing that most of the grains were cone shaped and their vertical angles and average diameter were around 120° and 105 μm, respectively.

3.2. Grinding conditions and procedure

Table 2 exhibits the grinding conditions. As the purpose of this work is predominantly to reveal the fundamental machining characteristics in UAG of Inconel 718 including the effects of the ultrasonic vibration and the wheel peripheral speed on the grinding force and specific

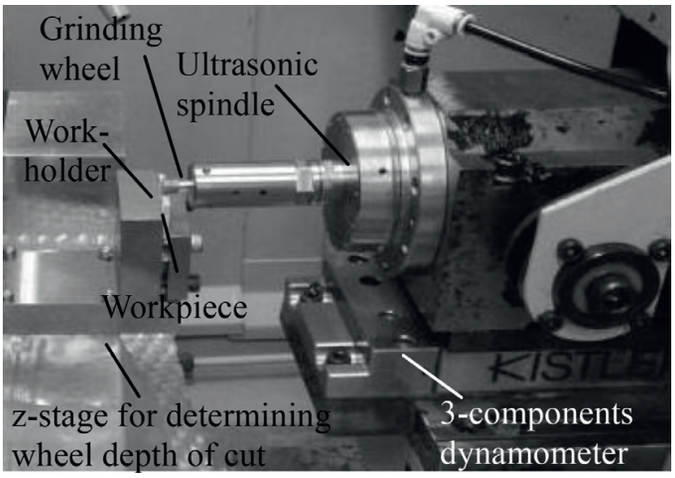

Figure 11. Photo of equipment for ultrasonic-assisted grinding.

Workpiece	Inconel 718, L48 mm × W36 mm × T3 mm
Grinding wheel	Electroplated cBN#140, φ8 × L8 mm (FSK 140)
Ultrasonic vibration	Frequency f = 40 kHz
	Amplitude $A_{P\text{-}P}$ = 0–9.4 μm
Process parameters	Workpiece feed rate V_w = 15 mm/min
	Wheel peripheral speed V_c = 100.5–138.2 m/min (wheel rotational speed n_g = 4000–5500 rpm)
	Grinding width b = 3 mm
	Wheel depth of cut Δ = 80 μm
Coolant	Without (dry grinding)

Table 2. Grinding conditions.

grinding energy, the work-surface finish, the chip formation (chip size and geometry), the material removal rate and the grinding wheel wear, the grinding operations were performed at different ultrasonic vibration amplitudes and wheel peripheral speeds but the constant workpiece feed rate and wheel depth of cut.

Typically, cBN abrasives require a cutting speed of over 50 m/min for grinding Inconel 718 [16]. Therefore, the value of wheel peripheral speed V_c was set at 100.5–138.2 m/min (wheel rotational speed n_g = 4000–5500 rpm). In order to ascertain the benefits from application of the ultrasonic vibration to precision grinding, the workpiece feed rate was set at a low value of 5 mm/min. Correspondingly, a large value of depth of cut is required to ensure material removal rate; hence, the value of Δ was set at 80 μm. The actual vibration amplitude A_{p-p} of the wheel was measured using the Laser Doppler vibrometer (LV-1610 by On Sokki Co., Ltd., Japan), revealing that the value of A_{p-p} was varied in a range of 0–9.4 μm as the power supplying level rises. In addition, dry grinding operations were performed without coolant supplying.

The material removal rate Q was also experimentally obtained using the relationship of $Q = b\Delta_r V_w$, where Δ_r is the actually measured work-depth removed. Furthermore, the ground work-surface roughness was measured with the surface profiler (Talysurf Intra by Taylor Hobson Inc.) to indicate the work-surface finish. For further investigation, the chips used for the SEM observation were those escaped out of the grinding zone during dry grinding and collected by a piece of conductive plastic (4×4 mm), which was located nearby the grinding zone. The working surface condition of grinding wheel, that is, the chips adhesion, the wheel wear behavior like grain releasing/fracture were also examined by SEM observation.

3.3. Fundamental grinding characteristics

Grinding force, specific grinding energy and material removal rate. Figure 12(a) and **(b)** shows the grinding forces measured under various values of A_{p-p} and V_c, respectively. Evidently, either the tangential force F_y or the normal one F_z monotonously decreased as the A_{p-p} increased (**Figure 12(a)**), and almost linearly decreased with the increasing V_c (**Figure 12(b)**). It should be noticed, for example, that at V_c = 138.2 m/min, once the ultrasonic vibration at A_{p-p} = 9.4 μm has been applied, the values of F_y and F_z were dropped by 51.9% and 38.6%, respectively, compared with that without ultrasonic vibration (A_{p-p} = 0 μm). Additionally, considered that the F_z affects tremendously, the formation of micro fracture defects on chip which is characterized by the knife chip, a lower F_z in UAG might lead to a smaller number of knife chips (see **Figures 18** and **19**) compared with that in CG.

In addition, the grinding force ratio of F_z/F_y was obtained as exhibited in **Figure 12**, showing that the ratio increased with the increasing A_{p-p} (**Figure 12(a)**), whereas little effect of the V_c can be observed on the ratio (**Figure 12(b)**) either in CG or in UAG. As revealed by Dong Kun Zhang [26], the lower friction ploughing and smaller chip deformation lead to the increase of grinding force ratio. Therefore, the results demonstrated that ultrasonic vibration contributed to the reduction of friction ploughing and chip deformation. Further, a larger vibration amplitude seemed to increase the material removal ratae, as shown in **Figure 13**. This confirmed that the ultrasonic vibration can enhance the material removal owing to the decrease in grinding forces.

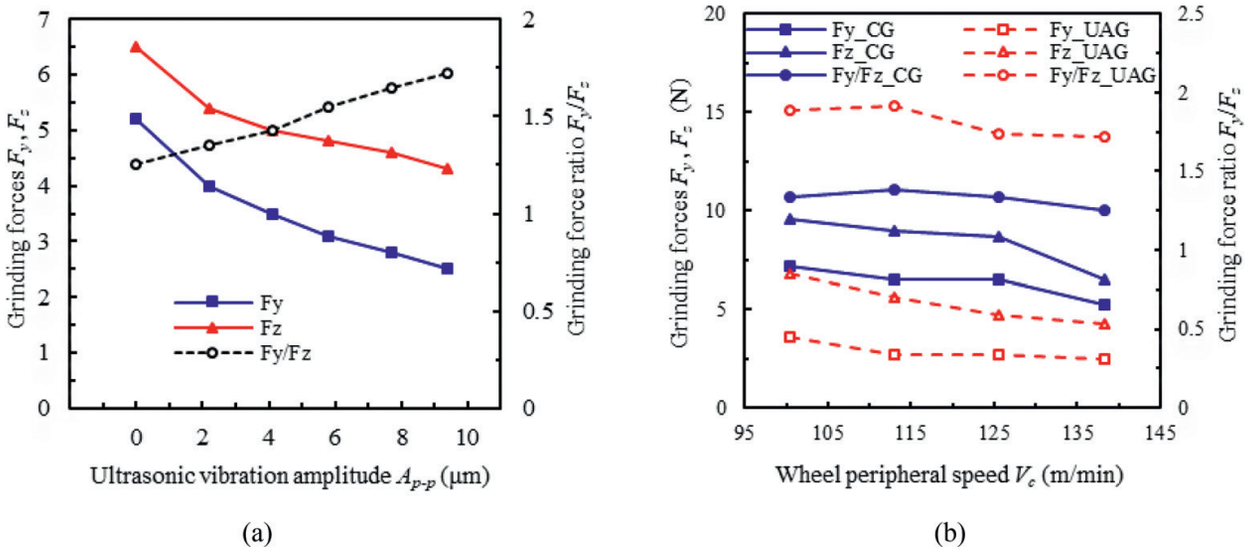

Figure 12. Effects of (a) vibration amplitude and (b) wheel peripheral speed on grinding forces.

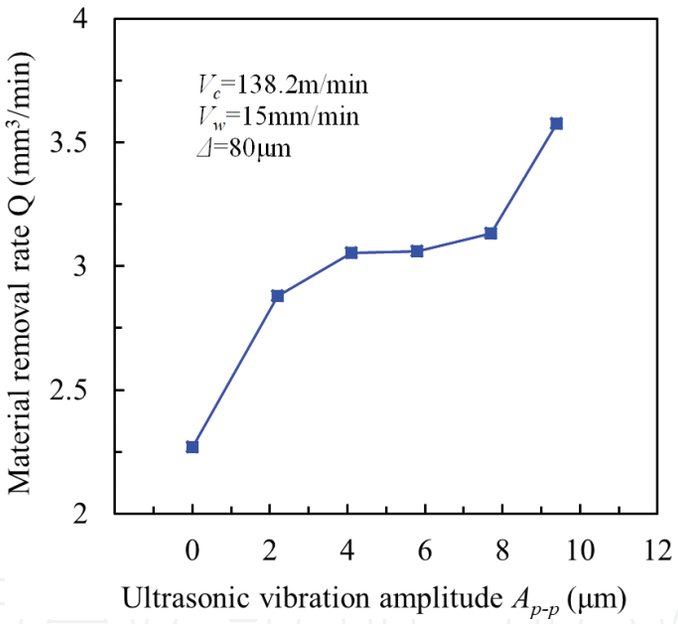

Figure 13. Effects of vibration amplitude on material removal rate.

Furthermore, the specific grinding energy, u, in UAG was compared with that in CG. As the u is defined as the energy per unit volume of material removed [27], it can be expressed in Eq. (1) in CG and Eq. (2) in UAG, respectively.

$$u = F_y V_c / 1000 b \Delta V_w \tag{1}$$

$$u = \left(F_y V_c + F_x V_x\right) / 1000 b \Delta V_w \tag{2}$$

where F_x (N) is the grinding force in x-direction due to the wheel ultrasonic vibration and V_x (m/min) is the wheel ultrasonic vibration speed determined by the equation of

$$V_x(t) = 2\pi f A_{p-p} \cos(2\pi f t) \tag{3}$$

Both of them are varied periodically at the frequency of f during grinding.

In the current work, the values of V_c, b, Δ and V_w have been already known as exhibited in **Table 2** and that of F_y is also the already known one as shown in **Figure 12**. The measured results of F_x and the calculated value of V_x are given in **Table 3**. The F_xV_x changed from 0 to the respective peek values for different A_{p-p}, while the F_yV_c decreased with the increase of A_{p-p}.

Figure 14 shows the relation between u and A_{p-p}. It can be seen from this figure that although the u varied between u_L and u_H at the given A_{p-p} for the sake of the ultrasonic vibration, the u intended to decrease as the A_{p-p} increases, confirming that the ultrasonic vibration benefits the reduction in the specific grinding energy significantly.

Work-surface finish. Given that the effective cutting edge distribution density affects the work-surface roughness in grinding processes and that this density is affected by the ultrasonic vibration [22], it was also investigated how the work-surface finish varied with vibration amplitude A_{p-p}. **Figure 15** shows the obtained results, demonstrating that the ultrasonic

A_{p-p} (mm)	0	2.2×10^{-3}	4.1×10^{-3}	5.8×10^{-3}	7.7×10^{-3}	9.4×10^{-3}
V_x (m/min)	0	−16.6–16.6	−30.9–30.9	−43.7–43.7	−58–58	−71–71
F_x (N)	0	−0.1–0.1	−0.1–0.1	−0.1–0.1	−0.1–0.1	−0.1–0.1
F_xV_x	0	0–1.7	0–3.1	0–4.4	0–5.8	0–7.1
F_yV_c	718.6	552.8	483.7	428.4	387.0	345.5

Table 3. V_x, F_x, F_xV_x and F_yV_c typically obtained at V_c = 138.2 m/min for various values of A_{p-p}.

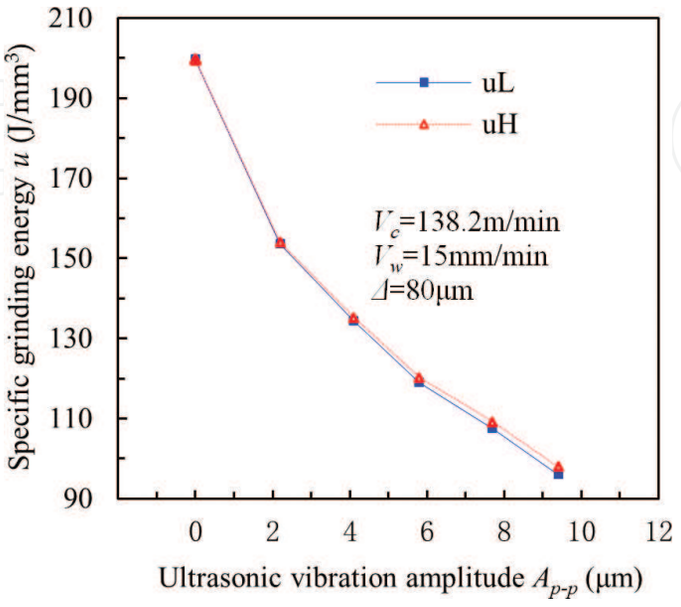

Figure 14. Effect of ultrasonic vibration on specific grinding energy.

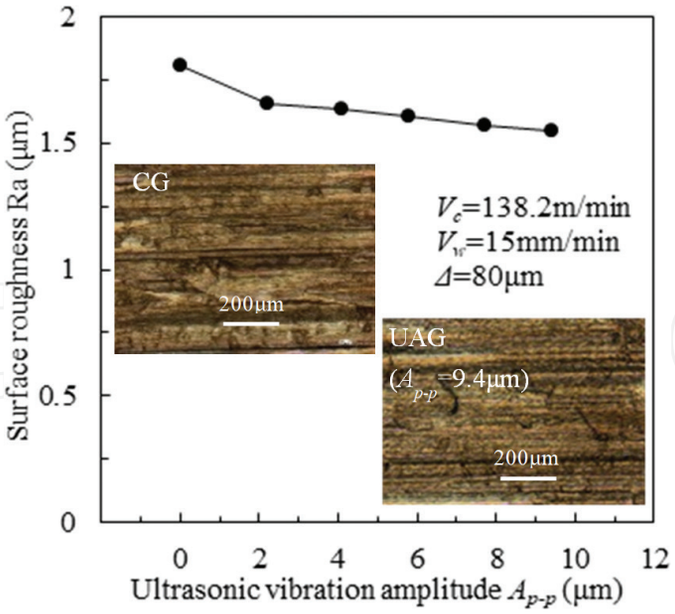

Figure 15. Effect of ultrasonic vibration amplitude on work-surface finish.

vibration indeed contributed to the work-surface finish improvement; the larger the A_{p-p} was, the smaller the work-surface roughness became. The optical microscopic images of work-surfaces in CG and UAG were also compared in the same figure, showing that on the work-surface by CG only parallel grain cutting marks were formed, whereas on that by UAG, many ultrasonic-induced knitting-patterned cutting marks overlap with the parallel ones.

Chips formed. An electron scanning microscope (SEM) with 3D measurement/observation functions (ERA-8900 by ELIONIX Co., Ltd.) was employed to measure the 3D chip size and observe the chip geometry. **Figure 16(a)** and **(b)** shows the 3D SEM images of chips formed in UAG (A_{P-P} = 9.4 μm) and CG at V_c = 138.2 m/min, respectively. The measured results of mean length and cross section area of chips are shown in **Figure 16 (c)** and **(d)**. It is evident in **Figure 16(c)** that the ultrasonic vibration leaded to the reduction of mean length and mean cross section area of chips. Especially, when the amplitude was A_{p-p} = 9.4 μm, the mean length was reduced by 36.3% and the cross section area was reduced by 64.3%. **Figure 16 (d)** shows the effect of the wheel peripheral speed V_c, demonstrating that as the V_c increases the cross section area intends to reduce either with or without ultrasonic vibration, but the effect on the chip length was not obvious.

In conventional grinding of Inconel 718, the formed chip could be classified into six types: flow, shear, rip, knife, slice and melt [28]. In this study, all the six types occurred; however, dominant types were shear, knife and flow either in CG or UAG as shown in **Figure 17**. Further, the number percentages of each type under different conditions were experimentally investigated, and the obtained results (**Figure 18**) show that the majority of chips in CG were shear type, whereas most of them in UAG were flow type especially at larger vibration amplitude (A_{p-p} ≥ 4.1 μm). This indicates that the UAG of Inconel 718 is potentially avoiding the formation of shear chips and prefers the flow chips especially at larger amplitude.

As for the effect of the wheel peripheral speed V_c, it can be found from **Figure 19** that in CG when the V_c changed from 100.5 m/min to 113 m/min, the percentage of the flow chip

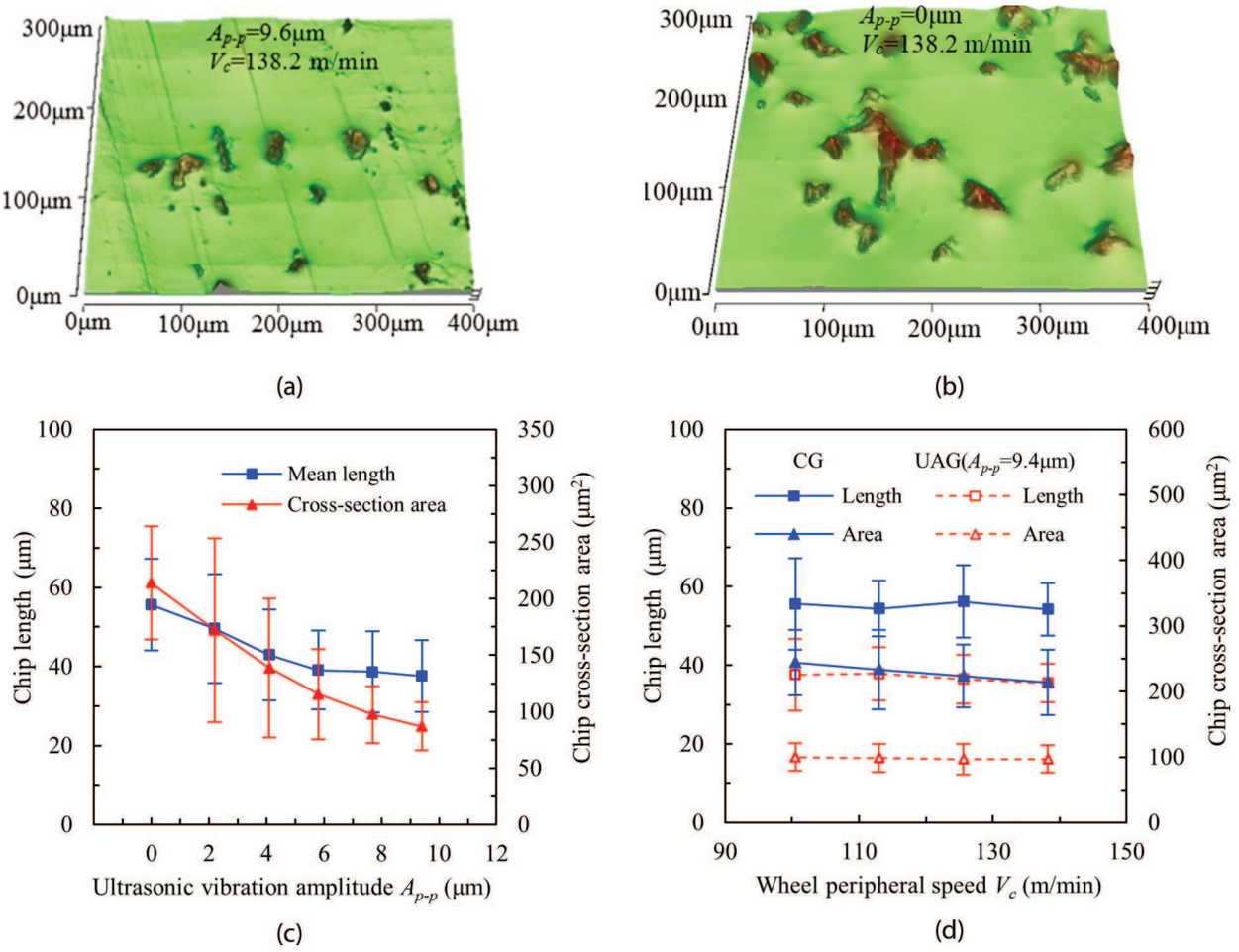

Figure 16. Effects of ultrasonic vibration and wheel peripheral speed on chip size: (a) 3D SEM images of chips in UAG at A_{p-p} = 9.4 μm, (b) 3D SEM images of chips in CG, (c) chip length and cross section area vs. vibration amplitude and (d) chip length and cross section area vs. wheel peripheral speed.

increased from 4 to 63% and the change in the percentage of knife chip was very small, while that of the shear chips reduced from 86 to 30%. As the increase of V_c the number percentage of three types of chips were not obvious. In UAG, the increase of V_c was not main effect to the change of number percentage of chips.

Working surface condition of grinding wheel. Through SEM observation, the working surface morphologies of wheel with/without ultrasonic vibration were captured. From the SEM images shown in **Figure 20**, it is found that both chips adhesion and grains releasing/fracture occurred during grinding. Comparing the right sides of **Figure 20(a)** and **(b)** revealed distinctly that the ultrasonic vibration reduced both the chips adhesion and grains releasing/fracture significantly.

Furthermore, the chips adhesion area was filtered, extracted and binarized by using Image-Pro Plus for quantitative analysis [22]. For this purpose, an observation zone with size of 1.13 mm × 6 mm on grinding wheel working surface was selected to measure the percentage of chips adhesion area in the total wheel working surface area, as shown in **Figure 21**. Obviously, increasing the ultrasonic amplitude leads to the reduction of the percentage of chips adhesion area. Especially, at A_{p-p} = 9.4 μm, a decrease by 72.4% was observed.

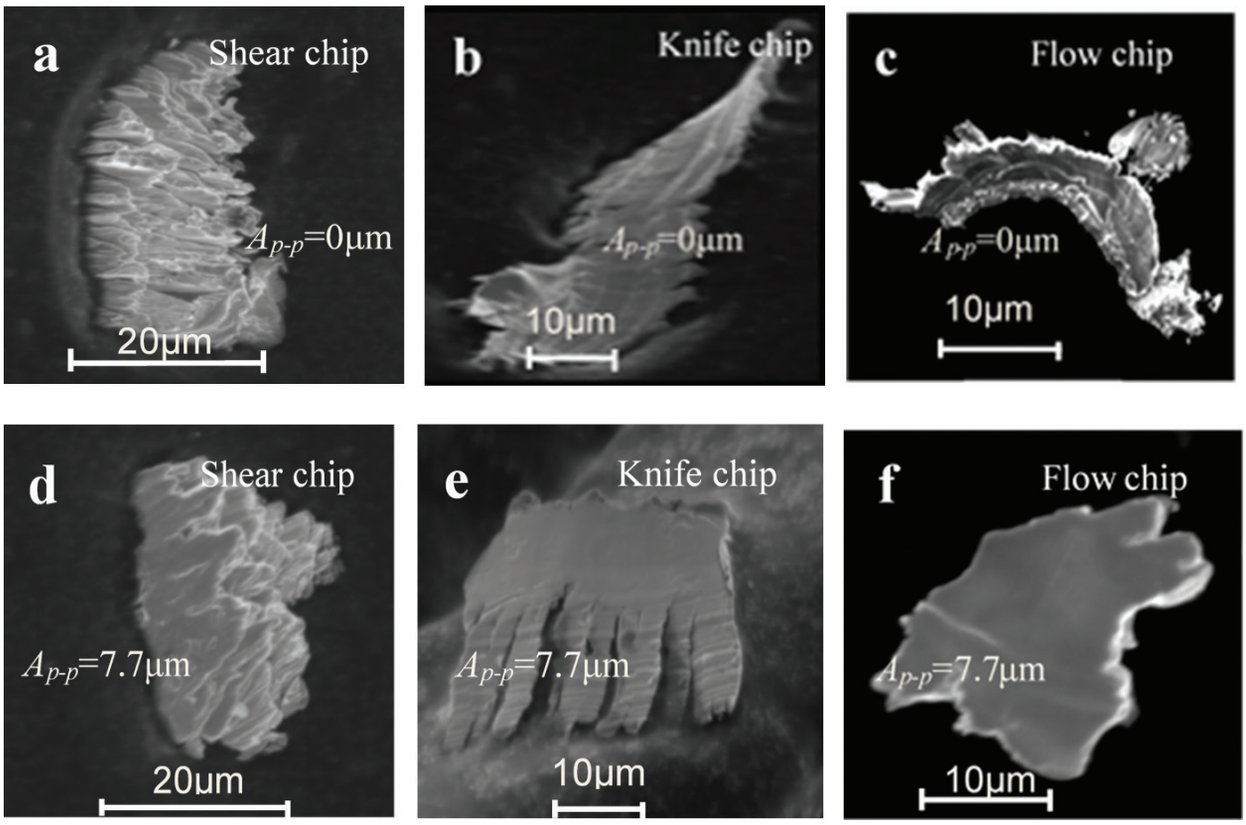

Figure 17. Chips type: (a) shear chip in CG; (b) knife chip in CG; (c) flow chip in CG; (d) shear chip in UAG; (e) knife chip in UAG and (f) flow chip in UAG, at Δ = 80 μm and V_c = 138.2 m/min.

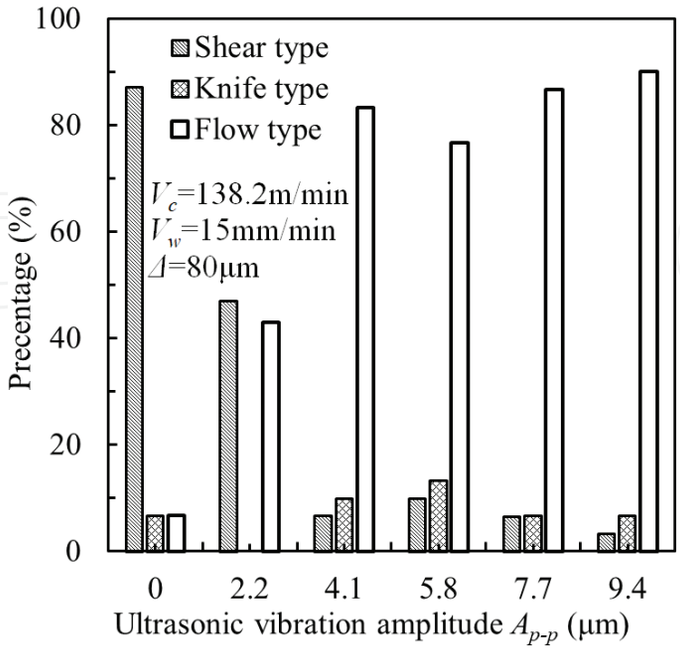

Figure 18. Effect of vibration amplitude on chip type.

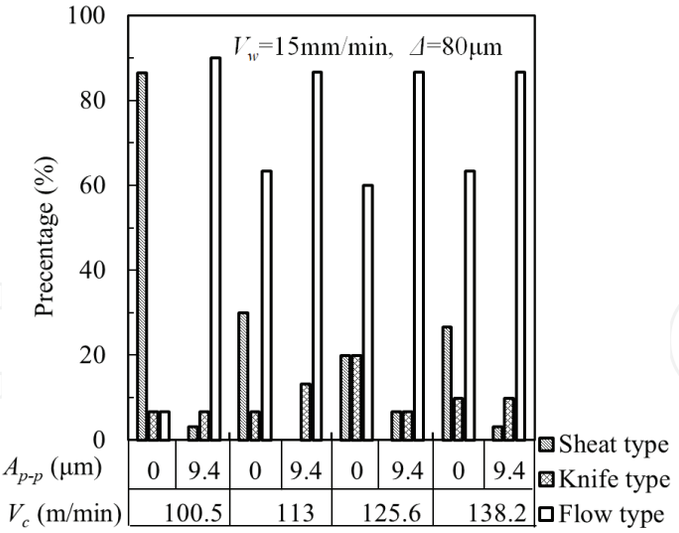

Figure 19. Effect of wheel peripheral speed on chip type.

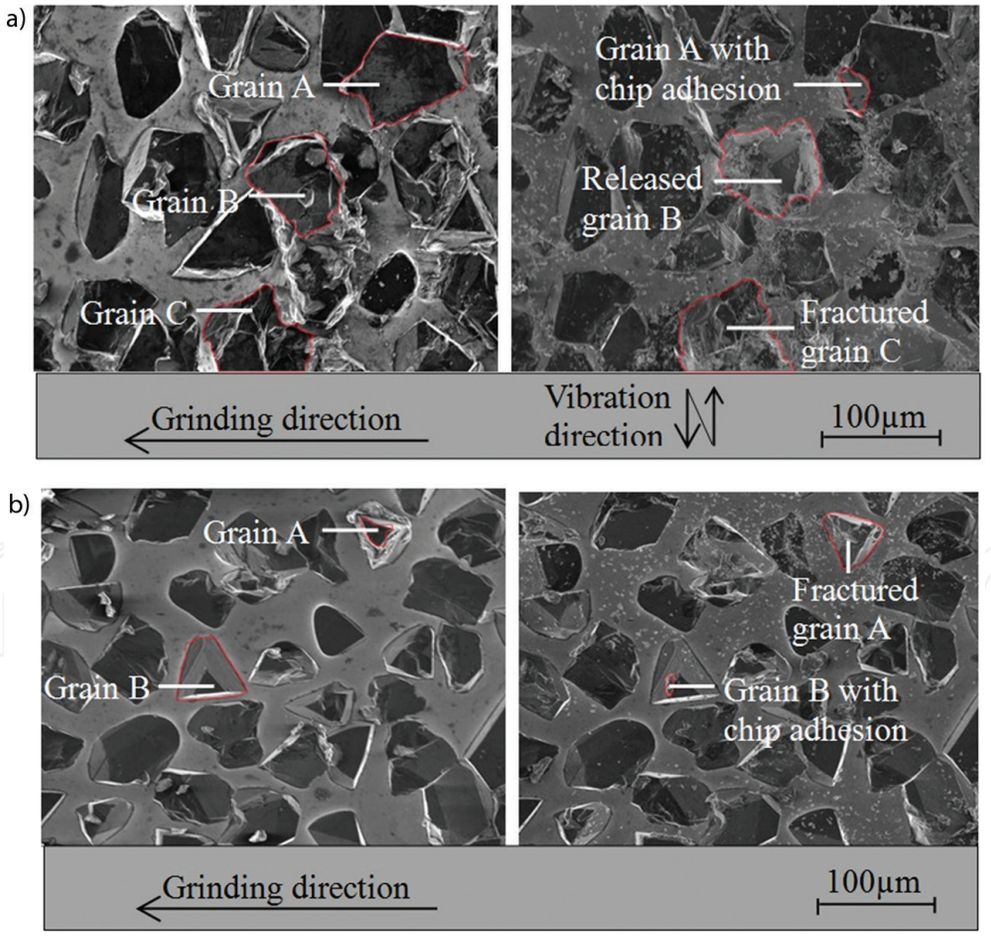

Figure 20. SEM images of the grinding wheel working surfaces before (left sides) /after (right sides) grinding of Inconel 718 (a) without and (b) with ultrasonic vibration: (a) in CG at A_{p-p} = 0 μm and V_c = 138.2 m/min and (b) in UAG at A_{p-p} = 9.4 μm and V_c = 138.2 m/min.

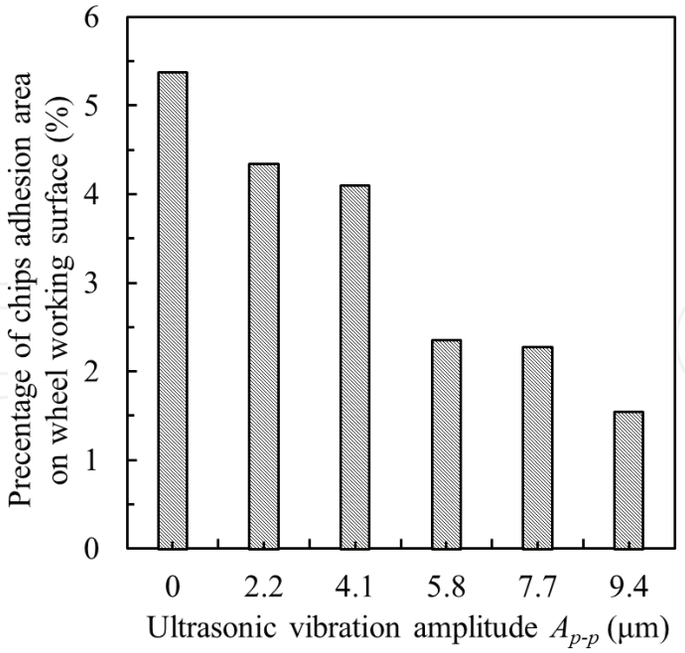

Figure 21. Effects of vibration amplitude on the percentage of chips adhesion area.

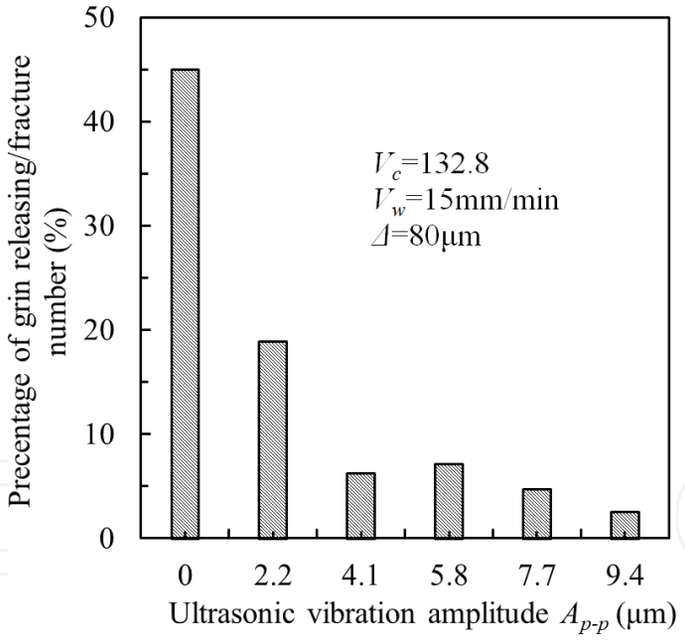

Figure 22. Effect of vibration amplitude on the percentage of grain releasing/fracture number.

At last, the releasing/fracture of abrasive grains was investigated by comparing the percentages of grain releasing/fracture number in total wheel working surface in CG and UAG, as shown in **Figure 22**. It is noticed that in CG (A_{p-p} = 0 μm), the percentage reached 44%. Once an ultrasonic vibration with a small amplitude of A_{p-p} = 2.2 μm has been imposed, the percentage turned to be less than 20%, demonstrating that the presence of ultrasonic vibration restraints

the grain releasing/fracture phenomenon considerably. In addition, when compared the CG result with the UAG one at $A_{p\text{-}p}$ = 9.4 μm, it is figured out that the percentage decreased by 40%. This phenomenon is attributed to the ultrasonic vibration-induced vertical inertia force which acts on chips. This vertical inertia force encourages chips to leave cutting edge and hence increases cutting capacity of grain.

4. Summary

As a step toward the development of a novel technique for the machining of superalloy Inconel 718, at first the elliptic ultrasonic-assisted turning (EUAT) method was proposed and its fundamental performance was experimentally confirmed, then the ultrasonic-assisted grinding of Inconel 718 was attempted and successfully elucidated the fundamental grinding characteristics. The obtained results can be summarized as following.

In EUAT, (1) the cutting force was considerably smaller than that in conventional turning (CT) and strengthening the ultrasonic vibration decreased the cutting force; (2) although ultrasonic vibration marks were formed on the work-surface along the cutting direction, the surface finish was improved, whereas scratches and pits obviously existed on the work-surface in CT and (3) the ultrasonic vibration significantly restrained the formation of built-up edge on cutting tool and decreased the flank wear of tool.

In UAG, (1) imposing the ultrasonic vibration to the grinding wheel decreased the grinding forces and increased the material removal rate significantly. Strengthening the wheel ultrasonic vibration decreased the specific grinding energy, demonstrating that the ultrasonic vibration benefits the reduction in the energy consumption. (2) The ultrasonic vibration contributed to the work-surface finish improvement; the larger the $A_{p\text{-}p}$ was, the work-surface roughness became better. (3) The chip size, that is, cross-section area and length, was distinctly affected by the ultrasonic vibration but little effect of wheel peripheral speed is observed. (4) The ultrasonic vibration in grinding is avoiding the formation of shear chips and prefers the flow chips especially at larger amplitude. (5) The grinding wheel wear was dominantly attributed to chips adhesion, grains releasing/fracture which are reduced significantly by the ultrasonic vibration. The percentage of chips adhesion area and the number percentage of grains released/fractured decreased as the vibration amplitude increased.

Author details

Yongbo Wu[1,2]*, Qiang Wang[1,2], Sisi Li[1,2] and Dong Lu[2]

*Address all correspondence to: wuyb@akita-pu.ac.jp

1 Akita Prefectural University, Akita, Japan

2 Southern University of Science and Technology, Shenzhen, China

References

[1] Thakur D, Ramamoorthy B, Vijayaraghavan L. A study on the parameters in high-speed turning of superalloy Inconel 718. Materials and Manufacturing Processes. 2009; **24**(4):497-503

[2] Zhou J, Bushlya V, Avdovic P, Ståhl JE. Study of surface quality in high speed turning of Inconel 718 with uncoated and coated CBN tools. The International Journal of Advanced Manufacturing Technology. 2012;**58**(1-4):141-151

[3] Lin S, Chung C, Cheng Y. Combination of ultrasonic vibration and cryogenic cooling for cutting performance improvement of Inconel 718 turning. AIP Conf. Proc. 2011; **1163**(1):1163-1168

[4] Nath C, Rahman M. Effect of machining parameters in ultrasonic vibration cutting. International Journal of Machine Tools & Manufacture. 2008;**48**:965-974

[5] Salje E, Mohlgan H. Fundamental dependencies upon contact lengths and results in grinding. CIRP Annals—Manufacturing Technology. 1986;**35**(1):249-253

[6] Cao J, Wu Y, Lu D, Fujimoto M, Nomura M. Material removal behavior in ultrasonic-assisted scratching of SiC ceramics with a single diamond tool. International Journal of Machine Tools and Manufacture. 2014;**79**:49-61

[7] Subramanian K, Ramanath S, Tricard M. Mechanism of material removal in the precision grinding of ceramic. ASME Journal of Manufacturing Science and Engineering. 1997;**119**(4A):1-19. DOI: 10.1115/1.2831181

[8] Muhammad R, Ahmed N, Roy A, Silberschmidt VV. Turning of advanced alloys with vibrating cutting tool. Solid State Phenomena. 2012;**188**:277-284

[9] Tsao CC, Chen CC, Chen GC, Chueh CA, Qiu YX, Hsu CY. Ultrasonic-assisted on the turning of Inconel 718 by Taguchi method. Advanced Materials Research. 2012;**579**:160-173

[10] Babitsky V, Kalashnikov A, Meadows A, Wijesundara A. Ultrasonically assisted turning of aviation materials. Journal of Materials Processing Technology. 2003;**132**(1):157-167

[11] Silberschmidt VV, Mahdy SMA, Gouda MA, Naseer A, Maurotto A, Roy A. Surface-roughness improvement in ultrasonically assisted turning. Procedia CIRP. 2014;**13**: 49-54

[12] Hsu C, Lin Y, Lee W, Lo S. Machining characteristics of Inconel 718 using ultrasonic and high temperature-aided cutting. Journal of Materials Processing Technology. 2008; **198**(1):359-365

[13] Wang Y, Lin B, Wang S, Cao X. Study on the system matching of ultrasonic vibration assisted grinding for hard and brittle materials processing. International Journal of Machine Tools and Manufacture. 2014;**77**:66-73

[14] Liang Z, Wu Y, Wang X, Zhao W. A new two-dimensional ultrasonic assisted grinding (2D-UAG) method and its fundamental performance in monocrystal silicon machining. International Journal of Machine Tools and Manufacture. 2010;**50**(8):728-736

[15] Mult HC, Spur IG, Holl SE. Ultrasonic assisted grinding of ceramics. Journal of Materials Processing Technology. 1996;**62**(4):287-293

[16] Pei ZJ, Ferreira PM, Kapoor SG, Haselkorn M. Rotary ultrasonic machining for face milling of ceramics. International Journal of Machine Tools and Manufacture. 1995; **35**(7):1033-1046

[17] Liu DF, Cong WL, Pei ZJ, Tang YJ. A cutting force model for rotary ultrasonic machining of brittle materials. International Journal of Machine Tools and Manufacture. 2012; **52**(1):77-84

[18] Zahedi A, Tawakoli T, Akbari J. Energy aspects and workpiece surface characteristics in ultrasonic assisted cylindrical grinding of alumina-zirconia ceramics. Archives of Civil and Mechanical Engineering. 2015;**90**:16-28

[19] Bhaduri D, Soo SL, Aspinwall DK, Novovic D, Harden P, Bohr S, Martin D. A study on ultrasonic assisted creep feed grinding of nickel based superalloys. Proceedings of the CIRP. 2012;**1**:359-364

[20] Lu D, Q Wang YW, Cao J, Guo H. Fundamental turning characteristics of Inconel 718 by applying ultrasonic elliptical vibration on the base plane. Materials and Manufacturing Processes. 2015;**30**(8):1010-1017

[21] Q Wang YW, J Gu DL, Ji Y, Nomura M. Fundamental machining characteristics of the in-base-plane ultrasonic elliptic vibration assisted turning of Inconel 718. Procedia CIRP. 2016;**42**:858-862

[22] S Li, Y Wu, M Fujimoto, M Nomura. Improving the working surface condition of electroplated cubic boron nitride grinding quill in surface grinding of Inconel 718 by the assistance of ultrasonic vibration. Journal of Manufacturing Science and Engineering. 2016;**138**:071008-071001-8

[23] Li S, Wu Y, Nomura M. Effect of grinding wheel ultrasonic vibration on chip formation in surface grinding of Inconel 718. International Journal of Advanced Manufacturing Technology. 2016;**86**:1113-1125

[24] Mitrofanov A, Ahmed N, Babitsky V, Silberschmidt V. Finite element analysis of ltrasonically assisted turning of Inconel 718. Journal of Materials Processing Technology. 2004;**153**:233-239. DOI: 10.1016/j.jmatprotec.2004.04.299

[25] Zhang X, Senthil Kumar A, Rahman M, Nath C, Liu K. Experimental study on ultrasonic elliptical vibration cutting of hardened steel using PCD tools. Journal of Materials Processing Technology. 2011;**211**(11):1701-1709

[26] Zhang DK, Li C, Jia D, Zhang Y. Investigation into engineering ceramics grinding mechanism and the influential factors of the grinding force. International Journal of Control and Automation. 2014;**7**(4):19-34

[27] Shaw MC. Principles of Abrasive Processing. Australia: Mech Chem Engng. Inst. Engrs; 1996

[28] Tso P-L. An investigation of chip types in grinding. Journal of Materials Processing Technology. 1995;**53**:521-532

IntechOpen